

High-order accurate discontinuous Galerkin simulation tool for cargo hold fires

Mark Lohry
Princeton University

FAA JUP
April 2016

Outline

- 1 Background
- 2 Discontinuous Galerkin method for buoyancy-driven flow
- 3 Cargo hold sample results
- 4 3D development

Motivation

- FAA requirement for alarms to go off within 60 seconds of fire ignition.
- Several different detection methods are generally used together, e.g. temperature, smoke/particulate, radiation, optical
- Their effectiveness is determined by the dynamics of a particular fire and their relative position.
- Accurate prediction of fire-induced flow in a cargo hold is a necessary first step to predicting detection capabilities.
- More reliable detection capabilities could potentially reduce false alarms.

B707 cargo geometry

- Experimental and computational data for B707 cargo fires available from work at Sandia and FAA Tech center.
- Current goal is to perform a direct comparison of those results with our new solver.

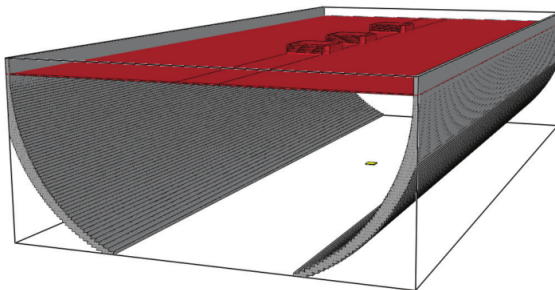


Figure : B707 cargo hold geometry.

Fire-induced fluid dynamics

- Detailed simulation of the combustion process is expensive and unnecessary; the large scale dynamics are primarily determined by the amount of heat release, its position, and the geometry.
- Commonly used models apply a heat source and input of reaction products (CO , CO_2 , etc.)

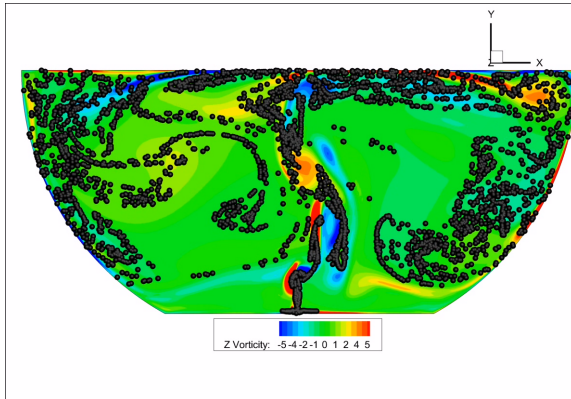


Figure : Flow driven by an enclosed heat source.

Cluttered geometry 2D

- A real fire is unlikely to happen in an empty cargo hold.
- Including some obstructions changes the flowfield considerably.

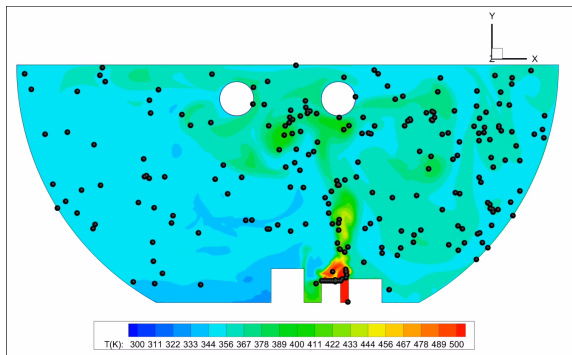


Figure : $t = 20\text{s}$ after ignition.

Simulation challenges

Simulating a single fire case is relatively straightforward, but of limited utility. There are several uncertainties to address:

- Initial position, size, and strength of a fire is unknown.
- Cargo hold geometry varies considerably depending on contents.

Simulation needs:

- Complex geometries: must handle complex boundary conditions accurately.
- Fast: uncertainty quantification will require a large number of simulations.
- Accurate: must accurately simulate vorticity-dominated turbulent flows for transport prediction.

Available tools

FDS: NIST's Fire Dynamics Simulator.

- **Pros:**

- Purpose-built for smoke and heat transport from fires using large eddy simulation.
- Combustion and radiation models.
- Built-in post-processing tools related to smoke transport.

- **Cons:**

- Handles complex boundaries with Cartesian cut cells: inaccurate for anything but rectangles.

OpenFOAM

- **Pros:**

- Similar combustion and radiation models to FDS, with additional thermodynamic models.
- Handles arbitrary body-fitted meshes.
- Wide array of LES models.

- **Cons:**

- Very slow for large cases.

Fluent

- **Pros:**

- Well known, full combustion and radiation modeling.
- Handles arbitrary body-fitted meshes.
- Wide array of LES models.

- **Cons:**

- Commercial

All limited to $O(\Delta x^2)$ accuracy.

High order accurate CFD

- Even very low intensity fires will have very complex flow phenomena poorly captured by low-order CFD methods.



Figure : Instability of smoke from a cigarette, *Perry & Lim, 1978*

High order accurate CFD

Order of accuracy in finite differences:

$$\begin{aligned}\frac{du}{dx} &\approx \frac{u(x + \Delta x) - u(x)}{\Delta x} + O(\Delta x) \\ \frac{du}{dx} &\approx \frac{u(x) - u(x - \Delta x)}{\Delta x} + O(\Delta x) \\ \frac{du}{dx} &\approx \frac{u(x + \Delta x) - u(x - \Delta x)}{2\Delta x} + O(\Delta x^2)\end{aligned}\tag{1}$$

- Error scales like $\sim O(\Delta x^n)$ for order n .
- For a 1st order method, halving the grid spacing reduces error by $\sim 1/2$.
- For a 4th order method, halving the grid spacing reduces error by $\sim 1/16$.

High order accurate CFD

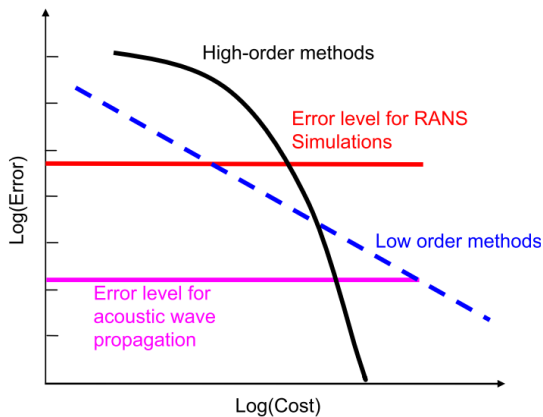


Figure : Generic error vs cost plot, Wang, 2007

Discretization method

For a multi-dimensional conservation law

$$\frac{\partial u(\mathbf{x}, t)}{\partial t} + \nabla \cdot \mathbf{f}(u(\mathbf{x}, t), \mathbf{x}, t) = 0 \quad (2)$$

approximate $u(\mathbf{x}, t)$ by

$$u(\mathbf{x}, t) \approx u_h(\mathbf{x}, t) = \sum_{i=1}^{N_p} u_h(\mathbf{x}_i, t) l_i(\mathbf{x}) = \sum_{i=1}^{N_p} \hat{u}_i(t) \psi_i(\mathbf{x}) \quad (3)$$

where $l_i(\mathbf{x})$ is the multidimensional Lagrange interpolating polynomial defined by grid points \mathbf{x}_i , N_p is the number of nodes in the element, and $\psi_i(\mathbf{x})$ is a local polynomial basis.

- Of the two equivalent approximations here, the first is termed *nodal* and the second *modal*. i.e., u_h represents values of u at discrete nodes with a reconstruction based on Lagrange polynomials, and \hat{u}_i represents modes/coefficients for reconstruction with the basis ψ_n .

Discretization method

Substituting the approximation u_h into the conservation law:

$$\frac{\partial u_h}{\partial t} + \nabla \cdot \mathbf{f}_h = 0$$

Integrate with a test function ψ_j , the same as used to represent the polynomial above,

$$\int_V \frac{\partial u_h}{\partial t} \psi_j \, dV + \int_V \nabla \cdot \mathbf{f}_h \psi_j \, dV = 0$$

Integration by parts on the spatial component:

$$\int_V \frac{\partial u_h}{\partial t} \psi_j \, dV - \int_V \nabla \psi_j \cdot \mathbf{f}_h \, dV + \oint_S \psi_j \mathbf{f}_h^* \cdot \mathbf{n} \, dS = 0$$

Using the modal representation, $u_h = \sum_{i=1}^{N_p} \hat{u}_i(t) \psi_i(\mathbf{x})$

$$\int_V \frac{\partial \hat{u}_i \psi_i}{\partial t} \psi_j \, dV - \int_V \nabla \psi_j \cdot \mathbf{f}_i \psi_i \, dV + \oint_S \psi_j \mathbf{f}_i^* \psi_i \cdot \mathbf{n} \, dS = 0$$

which gives the semi-discrete form of the classic modal DG method,

$$\mathbf{M}_{ij} \frac{d\hat{u}_i}{dt} = \int_V \nabla \psi_j \cdot \mathbf{f}_i \psi_i \, dV + \oint_S \psi_j \mathbf{f}_i^* \psi_i \cdot \mathbf{n} \, dS$$

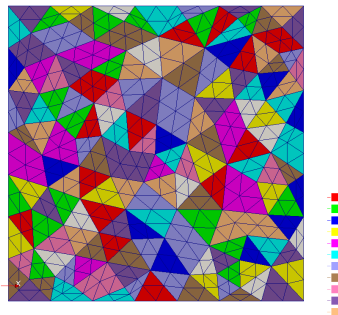
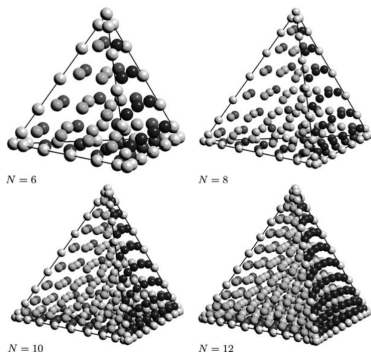
Here \mathbf{M} is the *mass matrix* (identity for orthonormal bases), \mathbf{n} the vector normal at an element surface, and \mathbf{f}^* is a conservative flux function at interfaces, equivalent to that used in finite volume methods.

Discretization method

The modal coefficients $\hat{\mathbf{u}}$ can always be represented on nodal locations \mathbf{u} through a change of basis by the *Vandermonde matrix*,

$$V\hat{\mathbf{u}} = \mathbf{u}$$

which turns the previous modal method into a nodal method. This code uses unstructured tetrahedral elements in 3D with Legendre-Gauss-Lobatto nodes:



(a) Volume nodes for varying order, Hesthaven & Warburton. (b) $N = 2$ element surfaces; nodes are at line intersections.

Discretization method - solving the discretized equations

This ends up with a potentially very large system of ODEs to be solved:

$$\frac{d\mathbf{u}}{dt} = \mathbf{f}(\mathbf{u}, \mathbf{u}', \mathbf{t})$$

Simplest method for integrating this system in time is the explicit (forward) Euler method:

$$\mathbf{u}^{n+1} = \mathbf{u}^n + \Delta t \mathbf{f}(\mathbf{u}, \mathbf{u}', \mathbf{t})^n$$

Unfortunately, explicit time-stepping for high-order DG is stable only for excessively small Δt ,

$$\Delta t = O\left(\frac{\Delta x}{N^2}\right)$$

where a mesh cell Δx can be very small (boundary layers, small geometric features) and N^2 quickly grows large. For any engineering-scale problem, explicit methods are unfeasible for use.

- This requires the use of implicit time-stepping methods, e.g. 1st order backward Euler:

$$\mathbf{u}^{n+1} = \mathbf{u}^n + \Delta t \mathbf{f}(\mathbf{u}, \mathbf{u}', \mathbf{t})^{n+1}$$

where we now have a set of non-linear equations to solve for \mathbf{u}^{n+1} . **Typically we use 3rd order or higher time-accurate schemes.**

Discretization method - solving the discretized equations

Task is to solve the very large non-linear system at each time step:

$$\mathbf{F}(\mathbf{u}) = 0$$

Newton's method for this problem derives from a Taylor expansion (Knoll/Keyes 2004):

$$\mathbf{F}(\mathbf{u}^{k+1}) = \mathbf{F}(\mathbf{u}^k) + \mathbf{F}'(\mathbf{u}^k)(\mathbf{u}^{k+1} - \mathbf{u}^k)$$

resulting in a sequence of linear systems

$$\mathbf{J}(\mathbf{u}^k)\delta\mathbf{u}^k = -\mathbf{F}(\mathbf{u}^k), \quad \mathbf{u}^{k+1} = \mathbf{u}^k + \delta\mathbf{u}^k$$

for the Jacobian \mathbf{J} .

- The linear system $\mathbf{J}(\mathbf{u}^k)\delta\mathbf{u}^k = -\mathbf{F}(\mathbf{u}^k)$ is straightforward enough to write, but for these methods \mathbf{J} is a very large sparse matrix which is prohibitively expensive to actually compute and store.
- A mesh of 100,000 4th order cells requires roughly 250GB of memory to store in 64-bit floats.

Discretization method - solving the discretized equations

- A remedy for this is to use a “Jacobian-Free” method based on Krylov subspace iterations (e.g. GMRES, BiCGSTAB), which only require the action of the jacobian in the form of matrix-vector products:

$$\mathbf{K} = \text{span}(\mathbf{J}\delta\mathbf{r}, \mathbf{J}^2\delta\mathbf{r}, \mathbf{J}^3\delta\mathbf{r}, \dots)$$

which can be approximated by a finite difference:

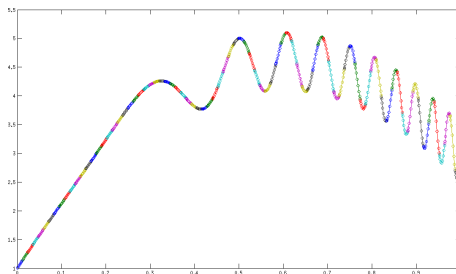
$$\mathbf{J}\mathbf{v} \approx [\mathbf{F}(\mathbf{u} + \epsilon\mathbf{v}) - \mathbf{F}(\mathbf{v})]/\epsilon$$

- This enables a solution method for the non-linear system that doesn't require ever explicitly forming the Jacobian, and instead only requires the evaluation of the RHS of the ODE.
- This is the *Jacobian-free Newton-Krylov* (JFNK) method:
 - Take a Newton step from the previous iterate.
 - Approximately solve the linear system using a matrix-free Krylov method.
 - Repeat until desired convergence is reached, and move to the next physical time step.
- Current solver uses a damped Newton line-search for the non-linear systems coupled with a GMRES Krylov method for the linear systems.

1D test case

1D Poisson test case to illustrate accuracy vs computational cost:

$$\frac{d^2 u}{dx^2} = -20 + a\phi'' \cos \phi - a\phi'^2 \sin \phi \quad (4)$$
$$a = 0.5, \phi(x) = 20\pi x^3$$



1D test case

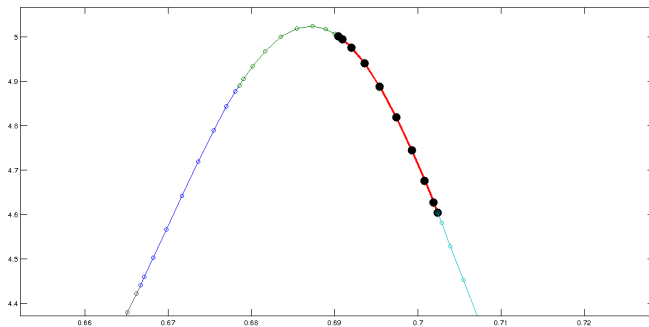


Figure : Close up of a single element with a 9th order polynomial basis.

1D test case

- For an ideal numerical method, computational cost is linearly proportional to the number of unknowns (degrees of freedom).
 - e.g. 10 cells with 10 quadrature nodes compared to 50 cells with 2 quadrature nodes.
- The end result is achieving equivalent accuracy with less computational expense or higher accuracy at similar computational expense compared to traditional finite volume methods.

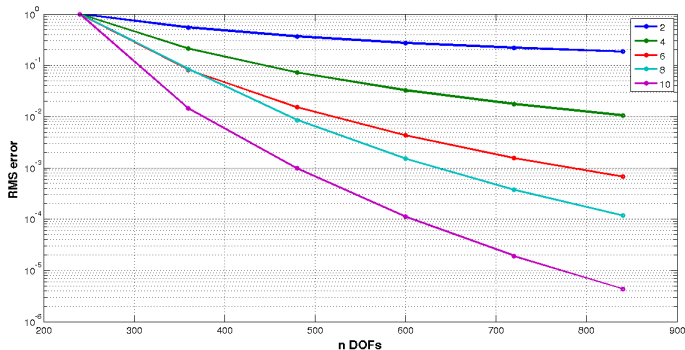
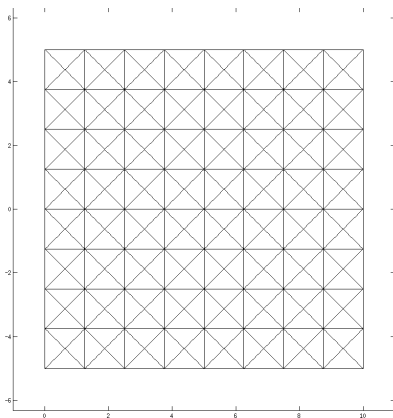
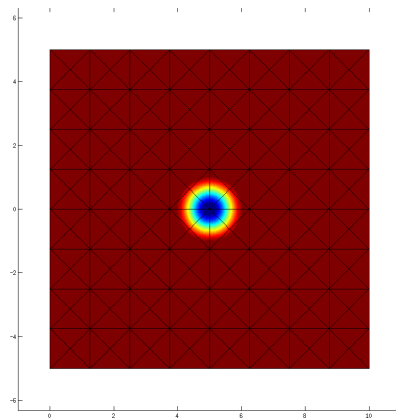


Figure : Error for varying order of accuracy with constant DOFs on 1D test case.

Test case - Isentropic vortex



(a) Coarse mesh for vortex case.



(b) Initial vorticity.

Test case - Isentropic vortex

- Non-dissipative vorticity convection is essential for these simulations.
- Test case of Yee et al (1999) for a convecting vortex is an exact solution for the compressible Euler equations. Free-stream conditions are

$$\rho = 1, u = u_{\infty}, v = v_{\infty}, p = 1$$

with an initial perturbation

$$(du, dv) = \frac{\beta}{2\pi} \exp\left(\frac{1-r^2}{2}\right) [-(y-y_0), (x-x_0)]$$

$$T = 1 - \frac{(\gamma-1)\beta^2}{8\gamma\pi^2} \exp(1-r^2)$$

$$\rho = T^{\frac{1}{\gamma-1}}$$

$$p = \rho^{\gamma}$$

for vortex center (x_0, y_0) , and distance from center $r = \sqrt{(x-x_0)^2 + (y-y_0)^2}$.

Test case - Isentropic vortex - 1st order (c.f. 2nd order FV)

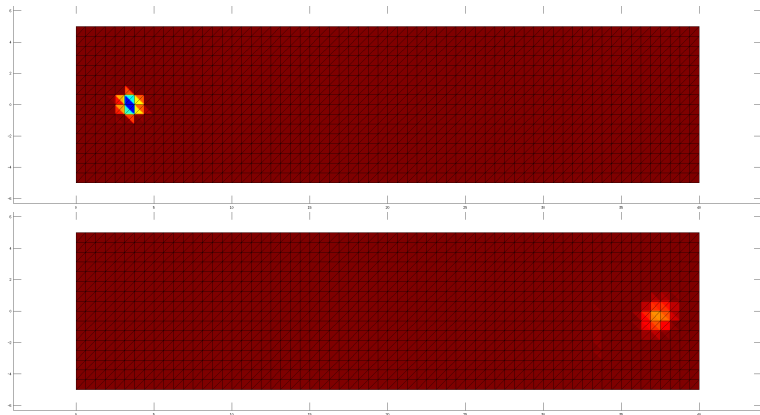


Figure : Vortex transport over 35 characteristic lengths, $O(\Delta x)$.

Test case - Isentropic vortex - 2nd order

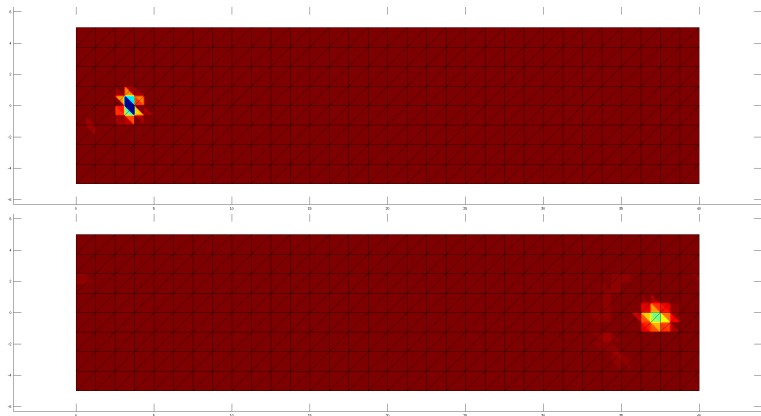


Figure : Vortex transport over 35 characteristic lengths, $O(\Delta x^2)$.

Test case - Isentropic vortex - 3rd order

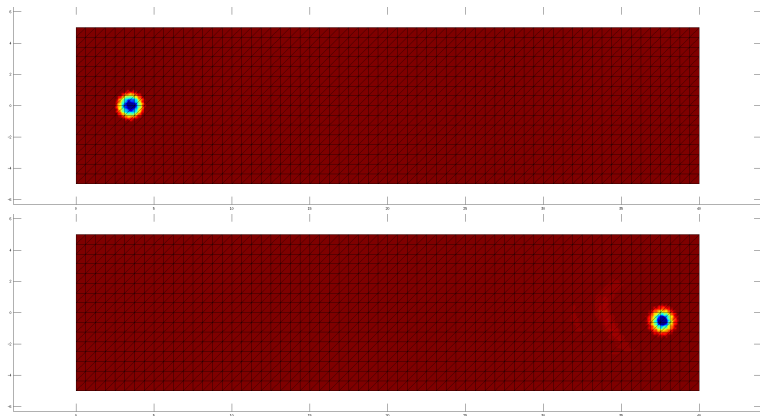


Figure : Vortex transport over 35 characteristic lengths, $O(\Delta x^3)$.

Test case - Isentropic vortex - 4th order

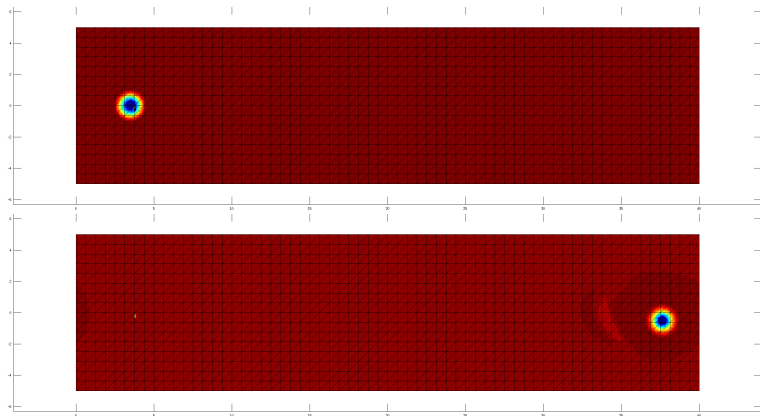


Figure : Vortex transport over 35 characteristic lengths, $O(\Delta x^4)$.

Test case - Isentropic vortex order of accuracy

- L_2 norm of kinetic energy losses for isentropic vortex convection.

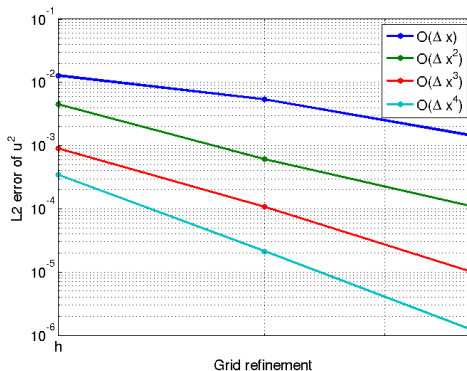


Figure : Solution accuracy versus grid refinement, for levels h , $h/2$, and $h/4$.

AIAA 2016 2D cargo hold results

Uncertainty Quantification for Cargo Hold Fires, DeGennaro, Lohry, Martinelli, & Rowley, *57th AIAA Structures, Structural Dynamics, and Materials Conference*, San Diego CA, Jan. 2016.

- Two objectives of this study:
 - Assess the feasibility of using DG methods for buoyancy-driven flows,
 - Use uncertainty quantification techniques to analyze statistical variations in flows.

AIAA 2016 2D cargo hold results

- The mock fire sources were chosen to vary based on 2 parameters: fire strength and location.
 - Fire location was chosen to vary between the centerline and the far right wall, exploiting the symmetry of the geometry.
 - Fire strength was chosen to vary between a weak, slowly rising plume and a faster rising plume.
- 5×5 parameter sweep performed for these 2 parameters.
- Simulations performed with 3rd order elements (10 nodes per 2D cell) with approximately 1,500 triangular cells, or 15,000 nodes. All boundary conditions are isothermal non-slip walls. Time integration by 3rd order backward difference formula (BDF).

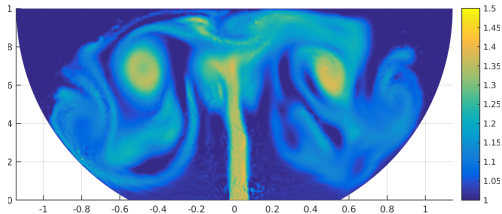


Figure : Flow driven by a heat source in a 2D cross-section. Colormap shown is temperature normalized by the initial bulk temperature.

AIAA 2016 2D cargo hold results

- Time evolution of temperature field:

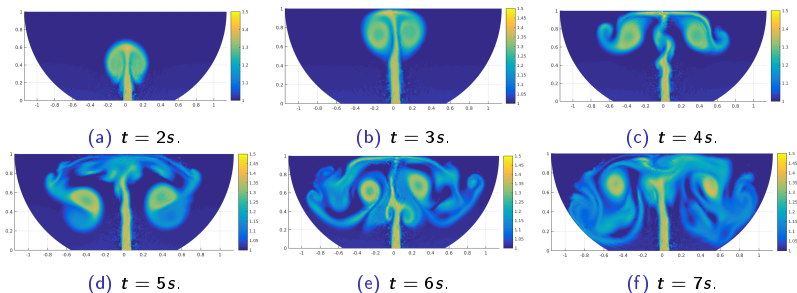


Figure : Temperature field time evolution for $T_s = 1.486$, $x_s = 0.024$ case.

AIAA 2016 2D cargo hold results

- Variation of fire source location:

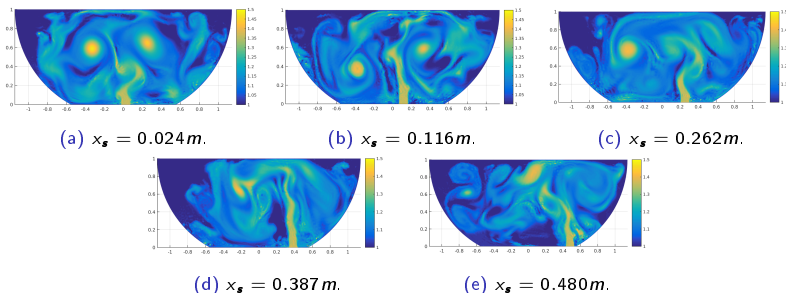


Figure : Temperature fields for $T_s = 1.486$ source at the 5 source locations, time $t = 10s$ after startup.

AIAA 2016 2D cargo hold results

- Variation of fire source temperature:

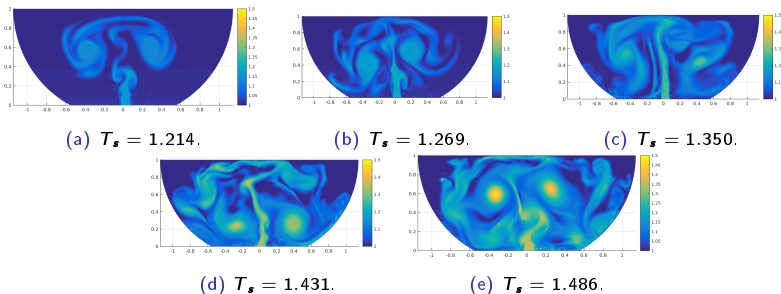


Figure : Temperature fields at $x_s = 0.024m$ for the 5 values of temperature source, time $t = 10s$ after startup.

AIAA 2016 2D cargo hold results

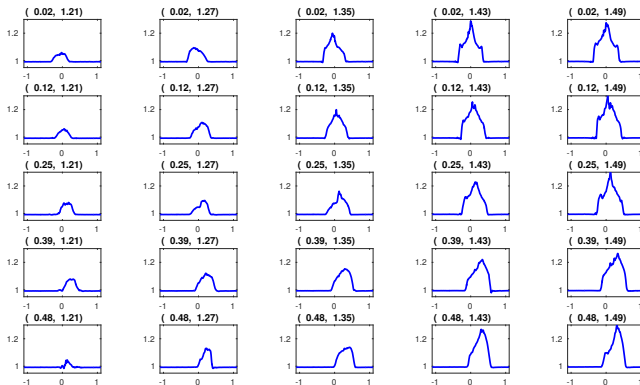


Figure : Time-averaged ceiling temperature distributions collected at the 25 quadrature nodes. Each subtitle corresponds to the parameter pair (x_s, T_s) .

3D isentropic vortex

- Current work is on verification and validation of the full 3D problem.

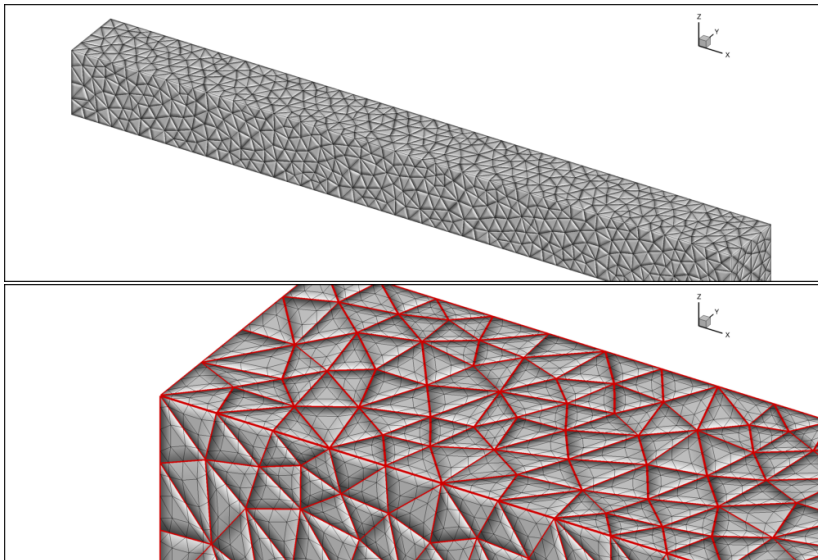
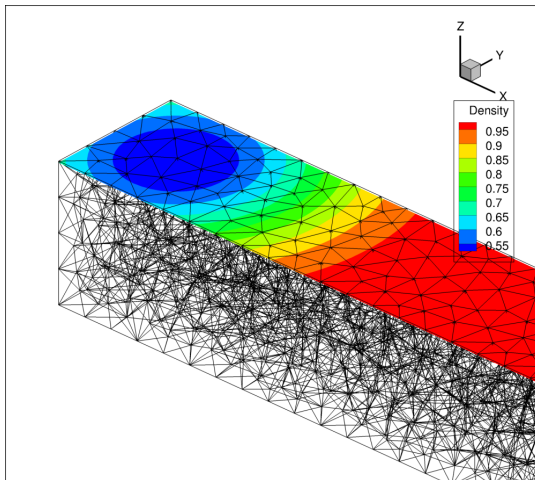


Figure : Comparison of mesh and 4th order elements.

3D isentropic vortex



3D isentropic vortex

Video

3D driven cavity

- Standard test case for viscous CFD. The “lid” of the cavity drives circulation through viscous entrainment similar to the buoyancy-driven instabilities.

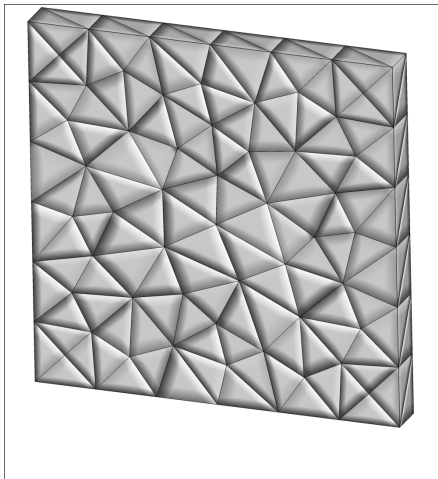


Figure : 354 cells 3D, 6x6x1 mesh.

3D driven cavity

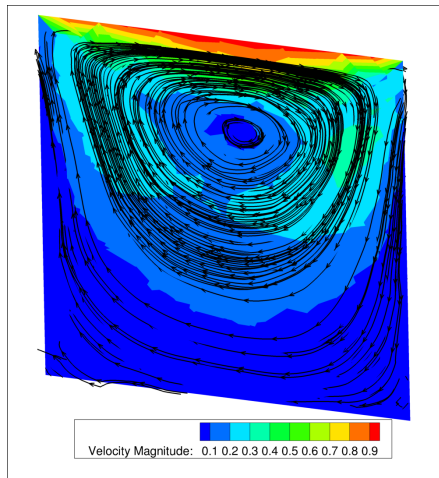


Figure : 1st order, 354 cells.

3D driven cavity

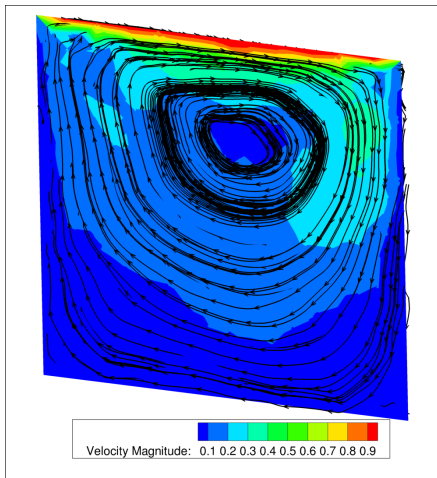


Figure : 2nd order, 354 cells.

3D driven cavity

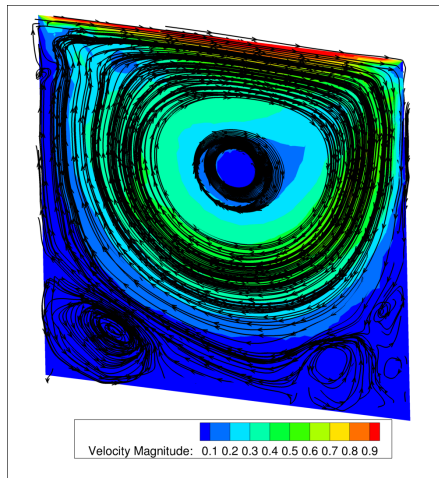


Figure : 3rd order, 354 cells.

3D driven cavity

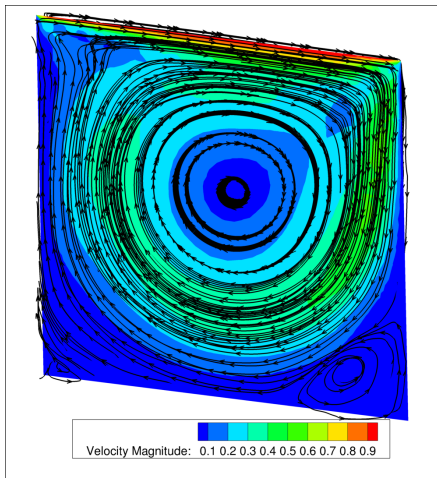


Figure : 4th order, 354 cells.

3D driven cavity

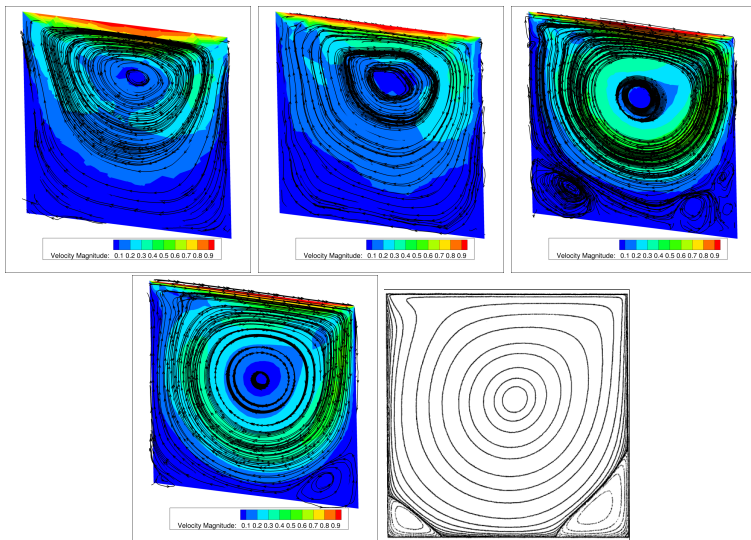


Figure : 3D DG solution with 354 cells c.f. Bruneau & Saad (2006), 1024×1024 grid.

Ongoing solver development

2D work completed:

- Established that high-order-accurate discontinuous Galerkin methods can be used for simulating buoyancy-driven flows such as those seen in cargo hold fires, using unstructured meshes suitable for arbitrary geometries.
- Demonstrated the use of these simulations in an uncertainty quantification framework to aid in fire sensor placement.

Current work is on extending this to a 3D solver for full cargo hold simulation:

- Functioning:
 - 3D unstructured flow solver, spatial discretization with arbitrary order of accuracy.
 - Parallel scaling.
 - Jacobian-Free Newton-Krylov for solution of non-linear algebra.
 - Implicit time integration for high order temporal accuracy and large time step stability.
 - 3D viscous effects
- Work in progress:
 - Full testing of 3D buoyancy-driven effects.
 - Implementation of Large Eddy Simulation (LES) models.
 - Full cargo hold simulations for validation.
 - Direct quantitative comparisons between OpenFOAM/FDS and this DG work for validation.